

Supporting information for

Time-release catalysis for cascade hydrolytic hydrogenation of cellulose

Junyan Fu ^a, Shihan Zhang ^a, Bingjie Qiu ^a, Richard Lee Smith, Jr ^b, Xinhua Qi^{a, *}

^a College of Environmental Science and Engineering, Nankai University, No. 38, Tongyan Road, Jinnan District, Tianjin 300350, China

^b Graduate School of Environmental Studies, Tohoku University, Aramaki Aza Aoba 468-1, Aoba-ku, Sendai 980-8572, Japan

Item	Page
Experimental Section	S3
Table S1. Detailed dosage of phosphorus source and hydrothermal conditions for synthesis of NiPO ₄ @POL- <i>t</i> and NiP@C- <i>x</i> samples.	S5
Fig. S1. FT-IR spectra of Fulvic acid (FA) and FA-Ni ²⁺ .	S6
Fig. S2. XRD patterns of solids containing NiPO ₄ precipitated at two different mixing times and conditions.	S7
Fig. S3. XRD patterns of (a) NiPO ₄ @POL-2 and (b) NiPO ₄ @POL-12 in FA solution. High-resolution XPS spectra of: (b) C 1s, (c) P 2p core-level spectra of NiPO ₄ @POL-2 and NiPO ₄ @POL-12 (NiPO ₄ @POL- <i>t</i> , <i>t</i> represents the hydrothermal reaction time at 200 °C).	S8
Fig. S4. XRD patterns of NiPO ₄ @POL-24 and NiPO ₄ (hydrothermal time: 24 h).	S9
Fig. S5. (a) Chemical reactions during reduction and carbonization of NiPO ₄ @POL-24 to NiP@C-3 under a hydrogen atmosphere, (b) Raman spectra of NiP@C-3 (I _D and I _G are the D-band and G-band Raman intensities).	S10
Fig. S6. (a) TEM image of NiP@C-3 and (b) particle size statistics of nanoparticles on the NiP@C-3 catalyst.	S11
Fig. S7. Characterization of NiP (a,b) SEM images, (c) TEM image, (d) HRTEM image; characterization of NiP/AC (e) TEM image, (f) HRTEM image (preparation detailed in supporting information).	S12
Fig. S8. (a) SEM image of NiP@C-3, inset: all elements overlapped mapping, (b) Map sum spectrum of NiP@C-3, (c) Elemental mapping for the same region of NiP@C-3 (C-red, O-green, P-violet and Ni-turquoise).	S13
Fig. S9. Contact angle of (a) NiP@C-3, (b) NiP/AC and (c) NiP.	S14
Fig. S10. XPS spectra of Ni 2p and P 2p of (a, b) NiP/AC and (c, d) NiP.	S15
Table S2. Content of XPS spectrum surface elements in prepared samples.	S16
Fig. S11. Arrhenius plots of glucose hydrogenation over NiP@C-3.	S17

E-mail: qixinhua@nankai.edu.cn (X. Qi).

Fig. S12. XPS spectra of Ni 2p and P 2p of (a, b) spent NiP/AC and (c, d) spent NiP.	S18
Fig. S13. TEM images of (a) spent NiP, (c) spent NiP/AC; HRTEM images of (b) spent NiP, (d) spent NiP/AC.	S19
Fig. S14. (a) TEM and (b) HRTEM image of spent NiP@C-3.	S20
Fig. S15. High-resolution XPS measurements of spent NiP@C-3, (a) Ni 2p and (b) P 2p.	S21
Fig. S16. XRD pattern of microcrystalline cellulose before and after ball milling.	S22
Fig. S17. Hydrolytic of untread and ball-milled cellulose in the deionized H ₂ O and H ₃ PO ₄ solution.	S23
Fig. S18. TEM diagram of catalyst for ball milling	S24
Fig. S19. NH ₃ -TPD profiles of NiP@C-3 catalyst.	S25
Fig. S20. HPLC chromatogram of cellulose conversion in deionized H ₂ O and catalyst leaching solution at 200 °C for 3 h.	S26
Fig. S21. Humins generated from cellulose hydrolysis in the 5 mL of deionized H ₂ O and catalysis leaching solution system.	S27
Table S3. Leaching phosphoric concentration and pH of cellulose reaction solution over the NiP, NiP@freeC and NiP@C-3 catalyst.	S28
Fig. S22. HPLC chromatogram of cellulose conversion over the NiP@C-3, NiP and NiP@freeC at 200 °C for 3 h.	S29
Fig. S23. Arrhenius plots of glucose degradation in the NiP catalysis system simulated by using pH=1.8 of H ₃ PO ₄ solution.	S30
Fig. S24 Arrhenius plots of glucose hydrogenation over the NiP.	S31
Fig. S25. Arrhenius plots of glucose degradation in the NiP@C-3 catalysis system simulated by using pH=3.1 of H ₃ PO ₄ solution	S32
Fig. S26. XRD pattern of spent NiP@C-3 and spent NiP.	S33
Fig. S27. Scheme of preparation, recycle, and regeneration of catalyst.	S34
Fig. S28. Catalytic performance for two catalyst-cellulose ratios.	S35
References	S36

Experimental Section

Preparation of NiP

10.8 mmol of $\text{Ni}(\text{NO}_3)_2 \cdot 6\text{H}_2\text{O}$ was dissolved in 80 mL of deionized water to prepare solution A, while 7.2 mmol of $(\text{NH}_4)_2\text{HPO}_4$ was dissolved in 20 mL of deionized water to prepare solution B. Solution B was then added drop by drop to solution A and stirred (600 rpm) at room temperature for 12 hours. The resulting mixture was transferred to a 200 mL high-pressure reactor with a Teflon lining and heated to 200 °C for 24 hours to produce NiPO_4 (the precursor of NiP). After washing and drying, NiPO_4 was reduced in a H_2 atmosphere by heating from room temperature to 600 °C at a rate of 2 °C·min⁻¹ and maintaining this temperature for 4 h to obtain NiP, with a Ni loading of 76.7 wt.% and a P loading of 21.2 wt.%.

Preparation of NiP/AC

NiP/AC was synthesized through precipitation onto activated carbon, resulting in a final composition of 29.5 wt.% Ni and 10.7 wt.% P. First, 10.8 mmol of $\text{Ni}(\text{NO}_3)_2 \cdot 6\text{H}_2\text{O}$ were dissolved in 80 mL of deionized water. To this solution, 0.65 g of activated carbon (C, Aladdin Reagent Co., Ltd.) was added. 7.2 mmol of $(\text{NH}_4)_2\text{HPO}_4$ (ammonium phosphate) was dissolved in 20 mL of deionized water. The $(\text{NH}_4)_2\text{HPO}_4$ solution was then slowly added to the solution containing activated carbon and nickel ions, resulting in the formation of NiPO_4/AC , the precursor to NiP/AC. After stirring the mixture at 600 rpm for 12 hours, it was washed and dried at room temperature. Finally, the solid was reduced in a hydrogen (H_2) atmosphere by heating from room temperature to 600 °C at a rate of 2 °C/min, and the temperature was maintained at 600 °C for 4 hours to obtain NiP/AC.

Preparation of NiP@freeC

NiP@C-3 was heated in a muffle oven at 400 °C under air atmosphere for 2 hours to remove the carbon and obtain the NiP@freeC catalyst.

DFT Calculation

The Vienna Ab Initio Package (VASP) was employed to perform the calculations based on the density functional theory (DFT) ¹⁻⁴. The interaction between the ion core and valence electron is described by using a projector augmented-wave (PAW) pseudopotential ^{5, 6}. The exchange-correlation interactions were treated by using the Perdew-Burke-Ernzerh of generalized gradient

approximation (GGA-PBE) formulation ⁷. The kinetic energy cutoff for the plane-wave expansion was set to 450 eV. Partial occupancies of the Kohn–Sham orbitals were allowed using the Gaussian smearing method and a width of 0.2 eV. The electronic energy was considered self-consistent when the energy change was smaller than 10⁻⁵ eV. A geometry optimization was done until the force was converged to 0.02 eV/Å⁻¹, respectively. Besides, the DFT-D3 method of Grimme was used for describing the dispersion interactions among all the atoms in adsorption models of interest ⁸.

NiP (001) facet model was constructed as a p (2×2) periodic slab of NiP bulk. NiP/AC contained a NiP cluster and a layer of graphene. The model of NiP encapsulated in one graphene shell consists of C₆₀ encapsulating a NiP cluster. A vacuum space of 15 Å is set along the z direction to ensure no interaction between adjacent images. During structural optimizations of the surface models, a 4×4×1 k-point mesh for Brillouin zone was used.

The reaction free energy change can be obtained with the equation below⁹:

$$\Delta G = \Delta E + \Delta E_{ZPE} - T\Delta S$$

where ΔE is the total energy difference before and after intermediate adsorbed, ΔE_{ZPE} and ΔS are, respectively, the differences of zero-point energy and entropy. The zero point energy and entropy of free molecules and adsorbents were obtained from the vibrational frequency calculations.

Determination of phosphate anion leaching

The leaching weight loss percentage was calculated by using the following formula:

$$\text{P leaching rate (\%)} = \frac{C_p * V}{m_p} \times 100\%$$

C_p was the P concentration (mg/L) in PO₄³⁻ solution after reaction detected by Ammonium molybdate spectrophotometric method, V was the volume of the reaction solution, m_p was the initial weight of P in fresh catalyst.

Recycle and reuse of P

An amount of 0.9 mL of ammonia solution (2.5~2.8 wt%) was added to 20 mL of post-reaction solution, containing 388 mg/L of P element, and stirred for 10 minutes to generate (NH₄)₂HPO₄, which is the phosphorus source for catalyst preparation. (NH₄)₂HPO₄ participating in catalyst preparation is described in detail part 2.2 of the text.

Table S1. Detailed dosage of phosphorus source and hydrothermal conditions for synthesis of NiPO₄@POL-*t* and NiP@C-*x* samples. Molar dosage of Ni(NO₃)₂ was fixed at 10.8 mmol.

Sample	(NH ₄) ₂ HPO ₄ dosage (mmol)	Molar ratio (P:Ni) for (NH ₄) ₂ HPO ₄ : Ni(NO ₃) ₂	Hydrothermal time (h)
NiPO ₄ @POL-2	7.2	6.6:10	2
NiPO ₄ @POL-12	7.2	6.6:10	12
NiPO ₄ @POL-24	7.2	6.6:10	24
NiPO ₄ @POL-48	7.2	6.6:10	48
NiP@C-1	1.08	1:10	24
NiP@C-2	3.6	3.3:10	24
NiP@C-3	7.2	6.6:10	24
NiP@C-4	32.4	30:10	24

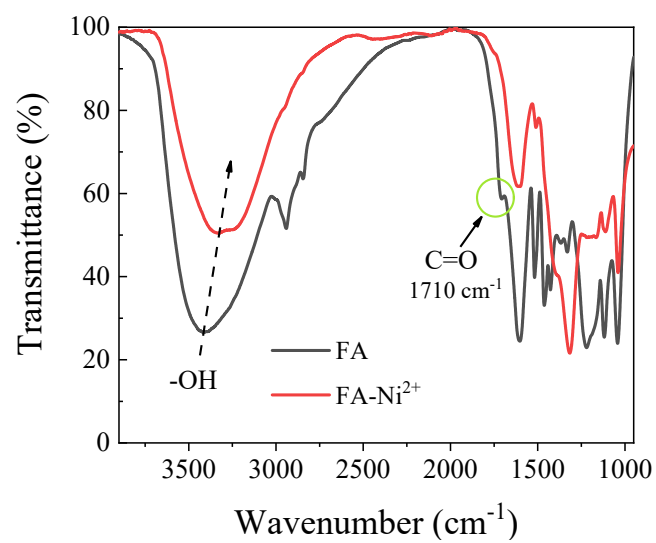


Fig. S1. FT-IR spectra of Fulvic acid (FA) and FA-Ni²⁺.

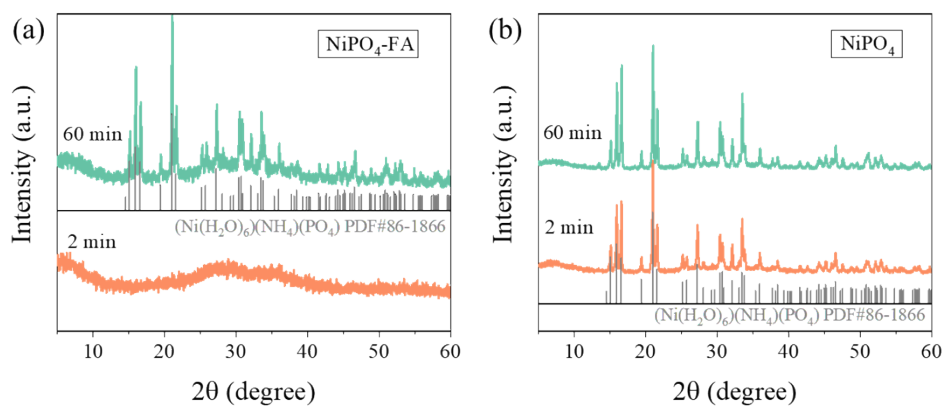


Fig. S2. XRD patterns of solids containing NiPO_4 precipitated at two different mixing times and conditions: (a) in fulvic acid (FA) solution ($\text{NiPO}_4\text{-FA}$) and (b) in deionized water (NiPO_4).

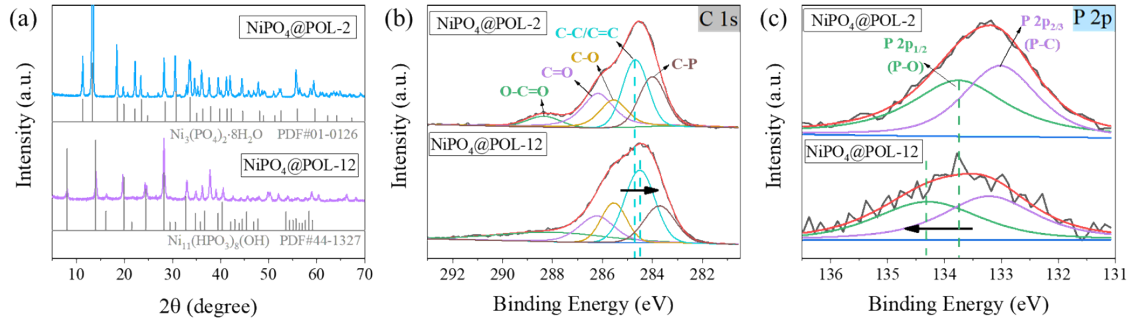


Fig. S3. XRD patterns of (a) $\text{NiPO}_4@\text{POL-2}$ and (b) $\text{NiPO}_4@\text{POL-12}$ in FA solution. High-resolution XPS spectra of: (b) C 1s, (c) P 2p core-level spectra of $\text{NiPO}_4@\text{POL-2}$ and $\text{NiPO}_4@\text{POL-12}$ ($\text{NiPO}_4@\text{POL-}t$, t represents the hydrothermal reaction time at 200 °C).

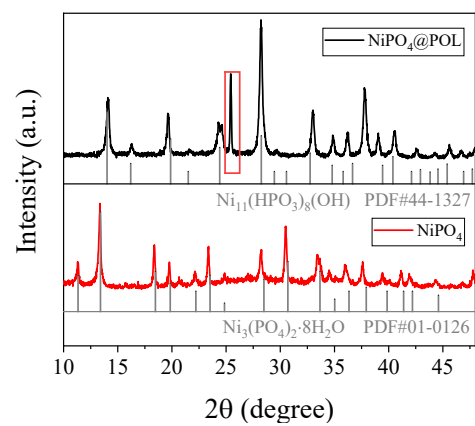


Fig. S4. XRD patterns of NiPO₄@POL-24 and NiPO₄ (hydrothermal time: 24 h).

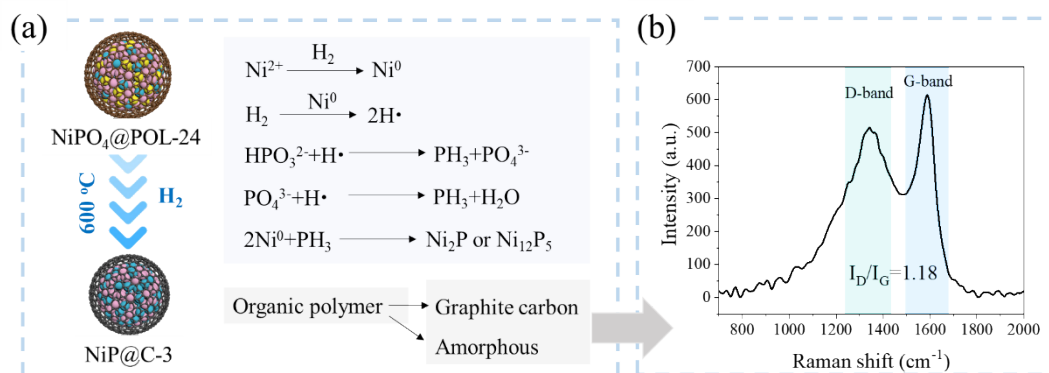


Fig. S5. (a) Chemical reactions during reduction and carbonization of NiPO₄@POL-24 to NiP@C-3 under a hydrogen atmosphere, (b) Raman spectra of NiP@C-3 (I_D and I_G are the D-band and G-band Raman intensities¹⁰).

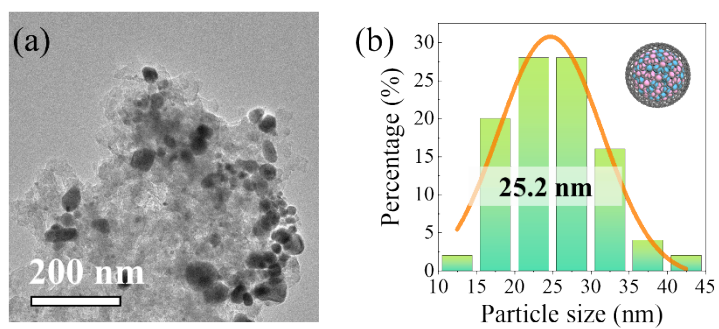


Fig. S6. (a) TEM image of NiP@C-3 and (b) particle size statistics of nanoparticles on the NiP@C-3 catalyst.

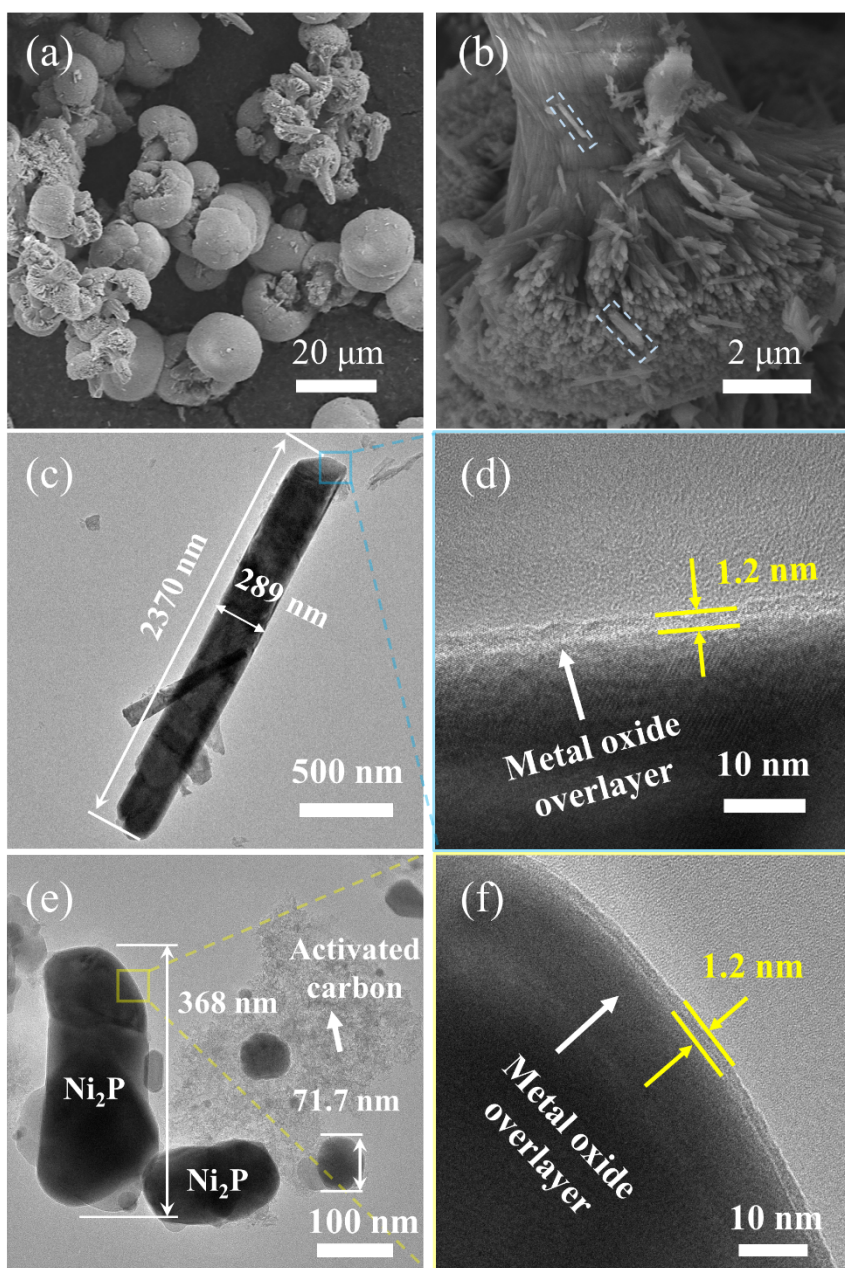


Fig. S7. Characterization of NiP (a,b) SEM images, (c) TEM image, (d) HRTEM image; characterization of NiP/AC (e) TEM image, (f) HRTEM image (preparation detailed in supporting information).

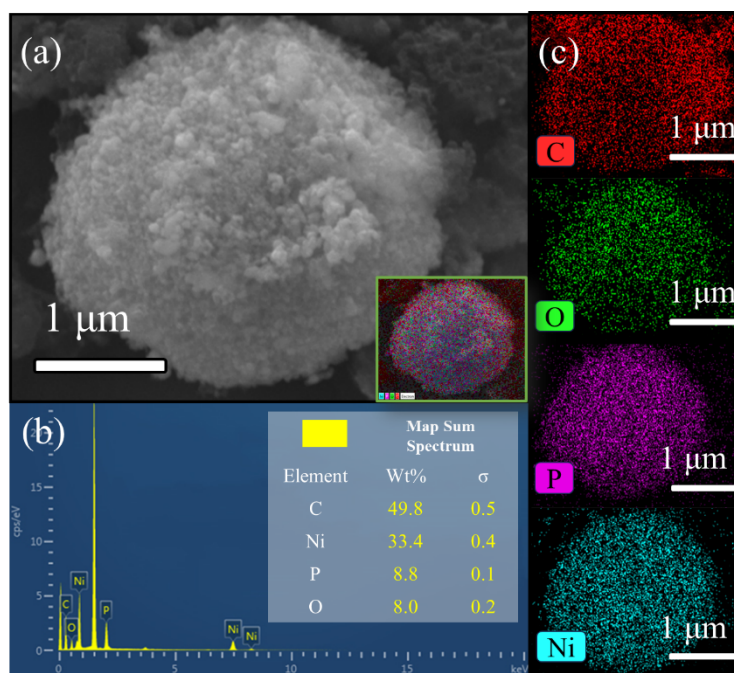


Fig. S8. (a) SEM image of NiP@C-3, inset: all elements overlapped mapping, (b) Map sum spectrum of NiP@C-3, (c) Elemental mapping for the same region of NiP@C-3 (C-red, O-green, P-violet and Ni-turquoise).

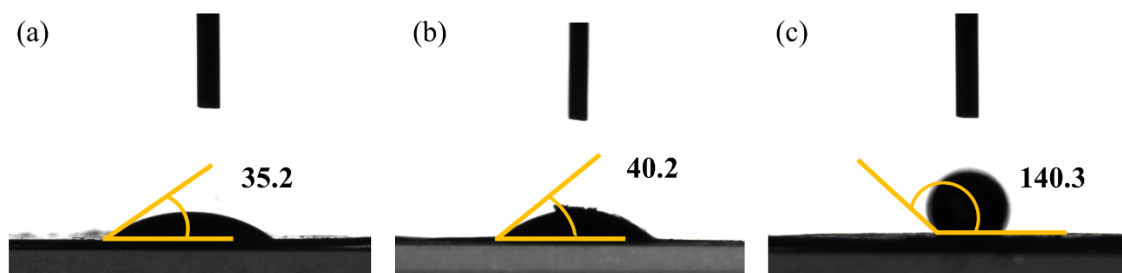


Fig. S9. Contact angle of (a) NiP@C-3, (b) NiP/AC and (c) NiP.

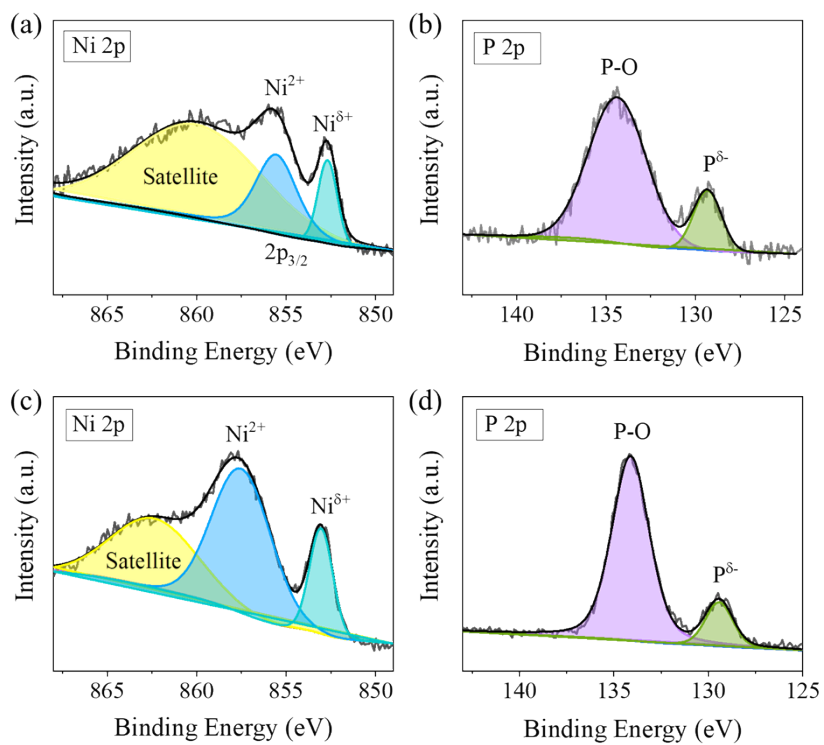


Fig. S10. XPS spectra of Ni 2p and P 2p of (a, b) NiP/AC and (c, d) NiP.

Table S2. Content of XPS spectrum surface elements in prepared samples.

Catalysts	Atomic conc. (%)			
	Ni ²⁺	Ni ^{δ+}	P-O	P ^{δ-}
NiP@C-3	38.7	61.3	62.8	31.8
NiP/AC	70.7	29.3	83.5	16.5
NiP	78.0	22.0	86.1	13.9

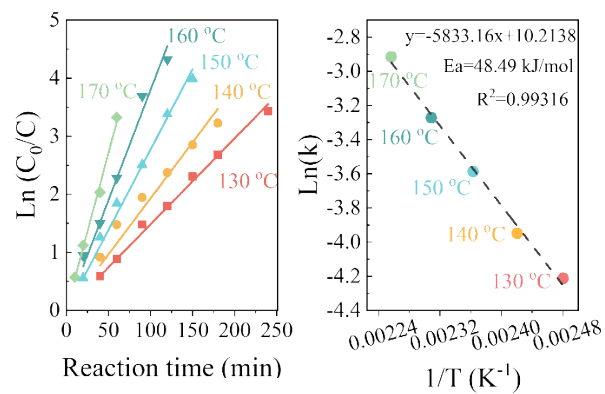


Fig. S11. Arrhenius plots of glucose hydrogenation over NiP@C-3. Reaction conditions: 3 MPa H_2 , 3 h, 10 g/L catalyst, 10 g/L glucose.

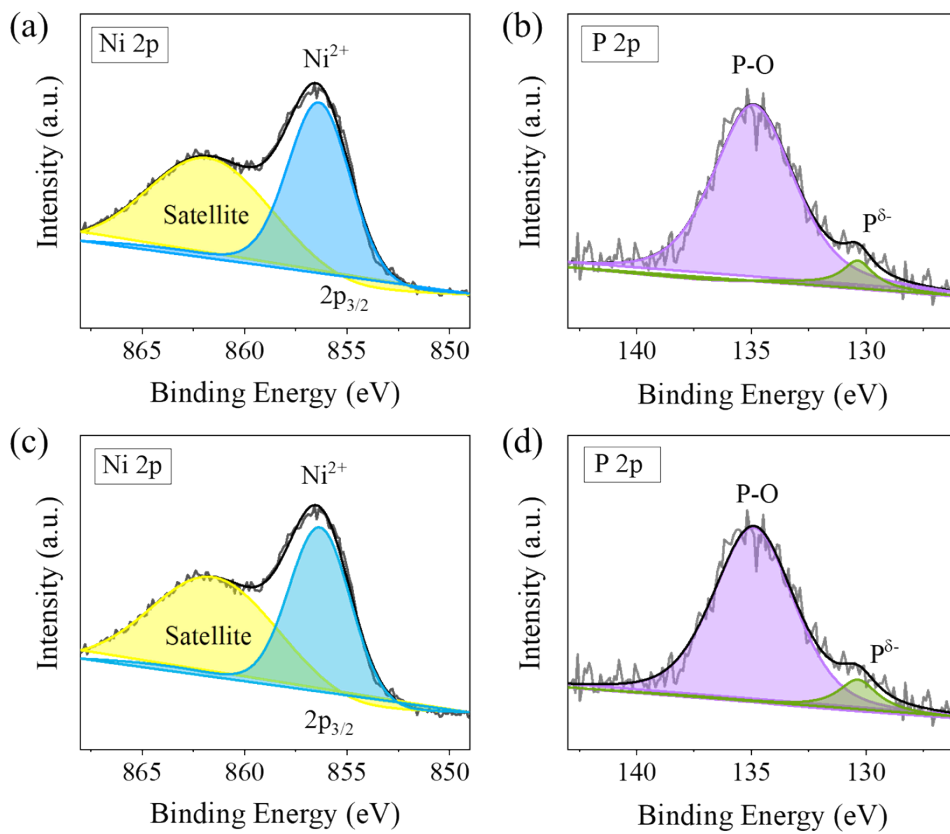


Fig. S12. XPS spectra of Ni 2p and P 2p of (a, b) spent NiP/AC and (c, d) spent NiP.

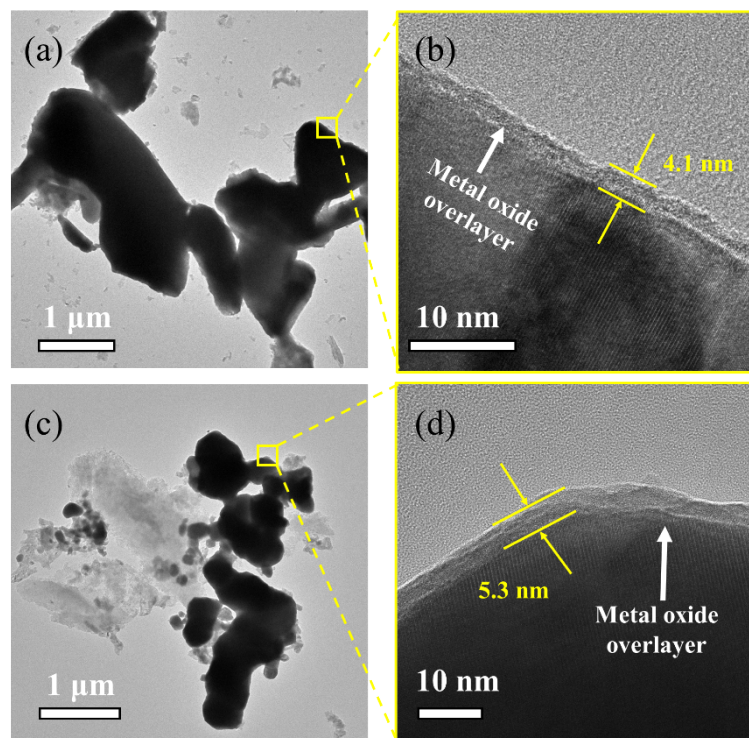


Fig. S13. TEM images of (a) spent NiP, (c) spent NiP/AC; HRTEM images of (b) spent NiP, (d) spent NiP/AC.

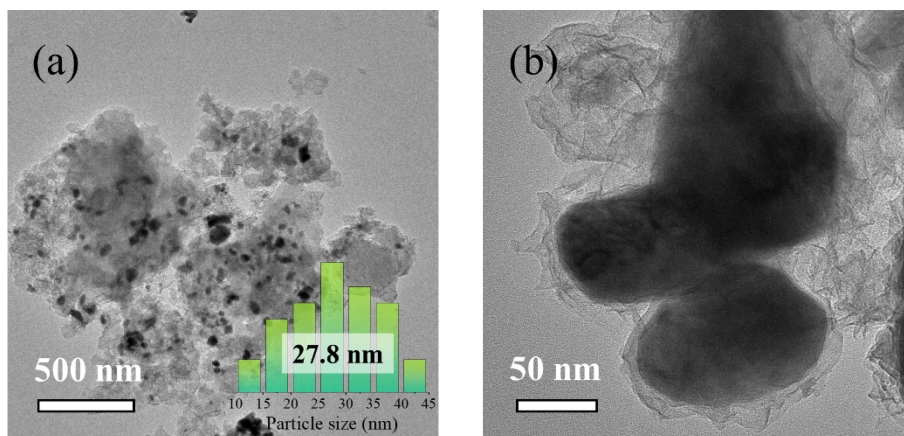


Fig. S14. (a) TEM and (b) HRTEM image of spent NiP@C-3.

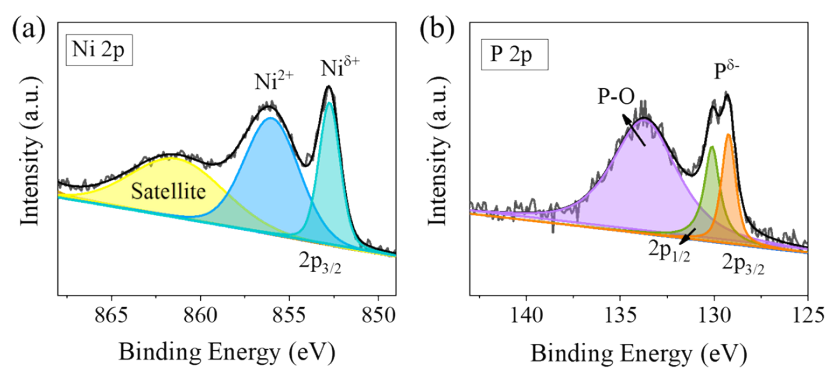


Fig. S15. High-resolution XPS measurements of spent NiP@C-3, (a) Ni 2p and (b) P 2p.

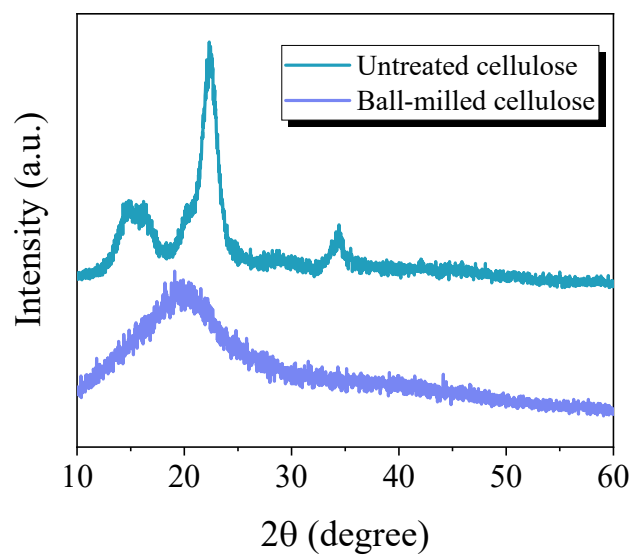


Fig. S16. XRD patterns of microcrystalline cellulose before and after ball milling.

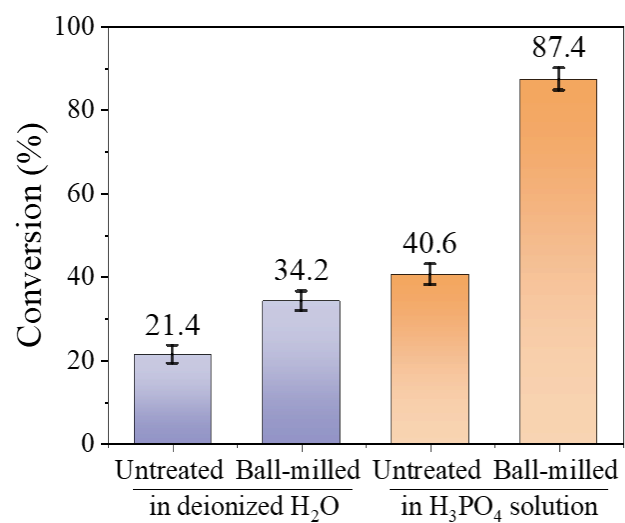


Fig. S17. Hydrolytic of untread and ball-milled cellulose in the deionized H₂O and H₃PO₄ solution.

Note: Ball milling can reduce the crystallinity of cellulose and increases the availability of acidic sites, especially in the homogeneous acid (phosphoric acid) catalytic process

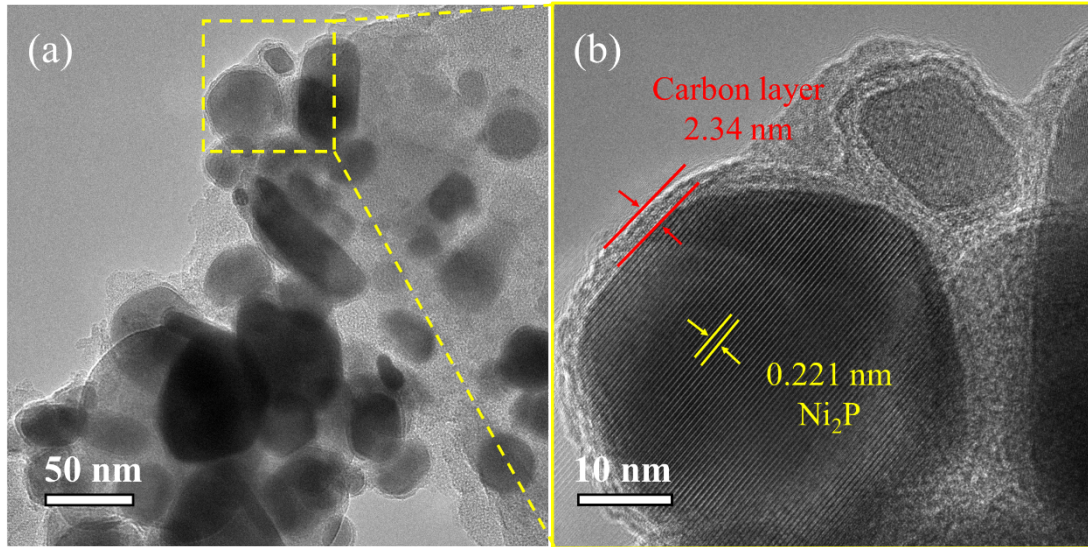


Fig. S18. (a) TEM diagram of catalyst for ball milling for 3 hours, (b) local high-resolution TEM image.

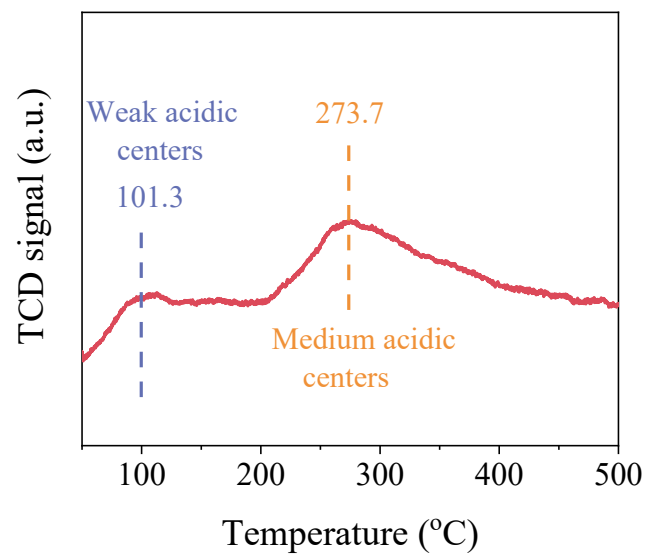


Fig. S19. NH₃-TPD profile of NiP@C-3 catalyst.

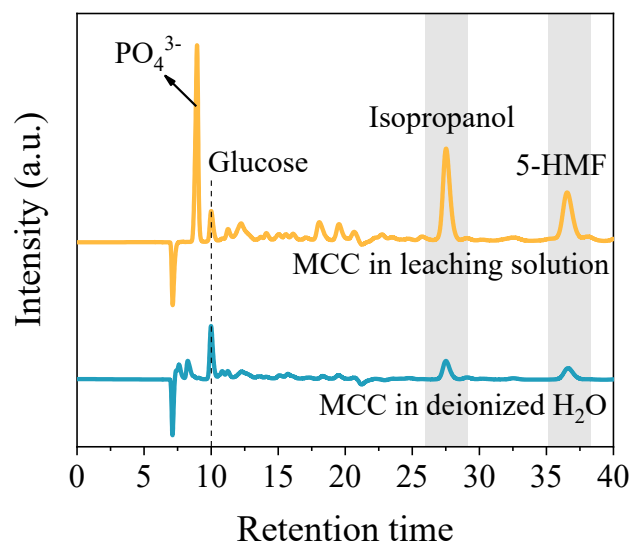


Fig. S20. HPLC chromatogram of cellulose conversion in deionized H₂O and catalyst leaching solution at 200 °C for 3 h.

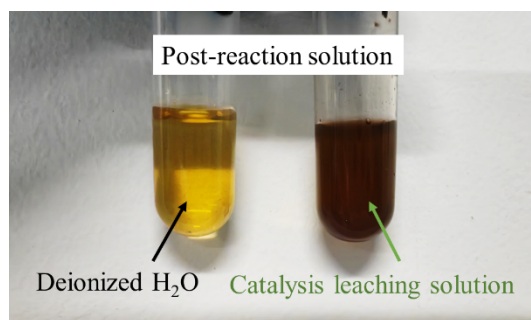


Fig. S21. Humins generated from cellulose hydrolysis in the 5 mL of deionized H₂O and catalysis leaching solution system (50 mg ball-milled cellulose, 200 °C, 3 h, 4MPa H₂).

Table S3. Leaching phosphoric concentration and pH of cellulose reaction solution over the NiP, NiP@freeC and NiP@C-3 catalyst.

Catalyst	Phosphate concentration (mg/L)	pH
NiP	663	1.83
NiP@freeC	682	1.75
NiP@C-3	389	3.09

Reaction condition: 50 mg catalyst and 50 mg cellulose mix milled, 5 mL deionized water, 4 MPa H₂, 200 °C for 3 h.

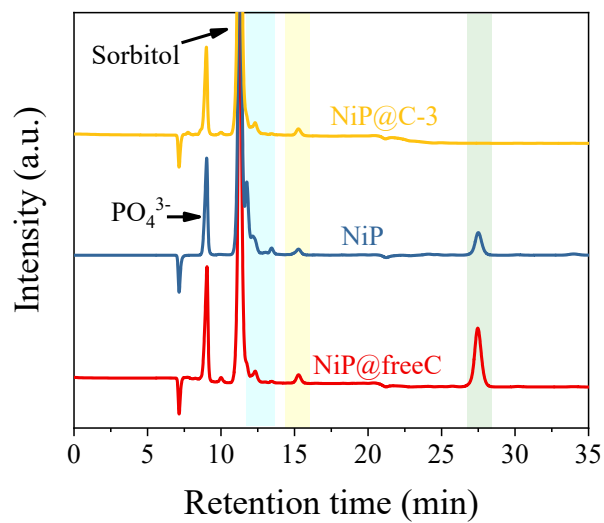


Fig. S22. HPLC chromatogram of cellulose conversion over the NiP@C-3, NiP and NiP@freeC at 200 °C for 3 h (reactant: microcrystalline cellulose, pretreatment method: mix milled).

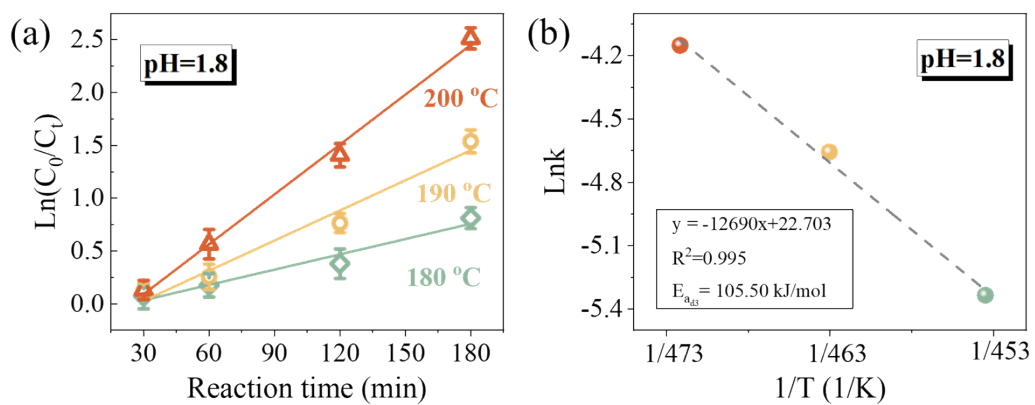


Fig. S23. Arrhenius plots of glucose degradation in the NiP catalysis system simulated by using pH=1.8 of H₃PO₄ solution (reaction condition: 5 mL H₃PO₄ solution, 10 g/L catalyst, 10 g/L glucose, 4MPa H₂).

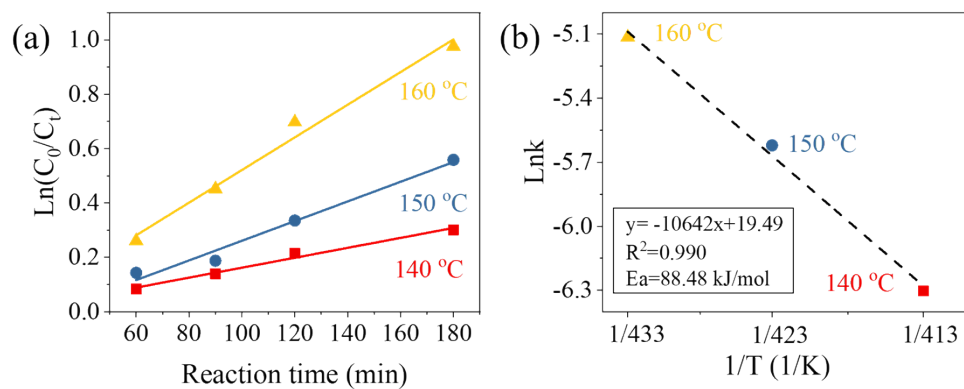


Fig. S24. Arrhenius plots of glucose hydrogenation over the NiP (reaction condition: 10 g/L catalyst, 10 g/L glucose, 3MPa H₂).

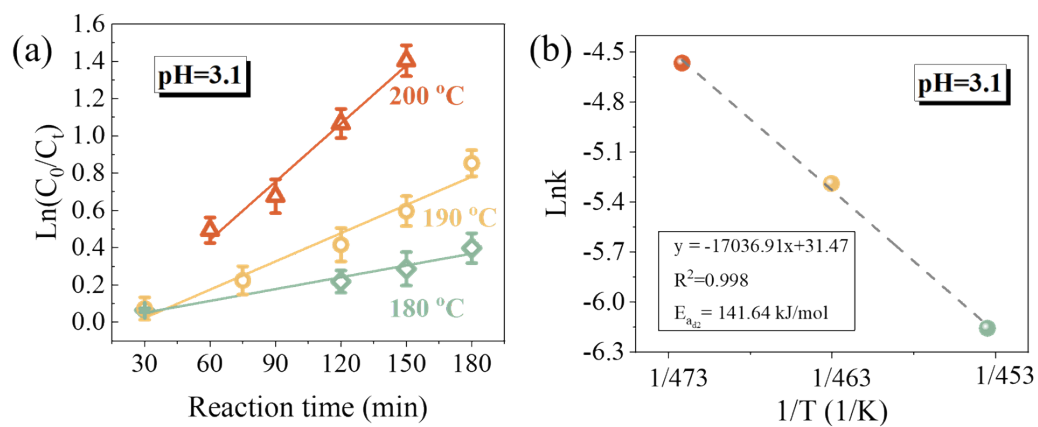


Fig. S25. Arrhenius plots of glucose degradation in the NiP@C-3 catalysis system simulated by using pH=3.1 of H₃PO₄ solution (reaction condition: 5 mL H₃PO₄ solution, 10 g/L catalyst, 10 g/L glucose, 3MPa H₂).

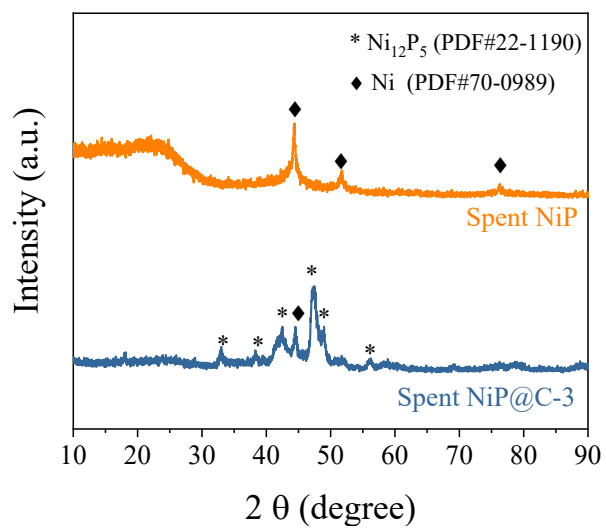


Fig. S26. XRD patterns of spent NiP@C-3 and spent NiP.

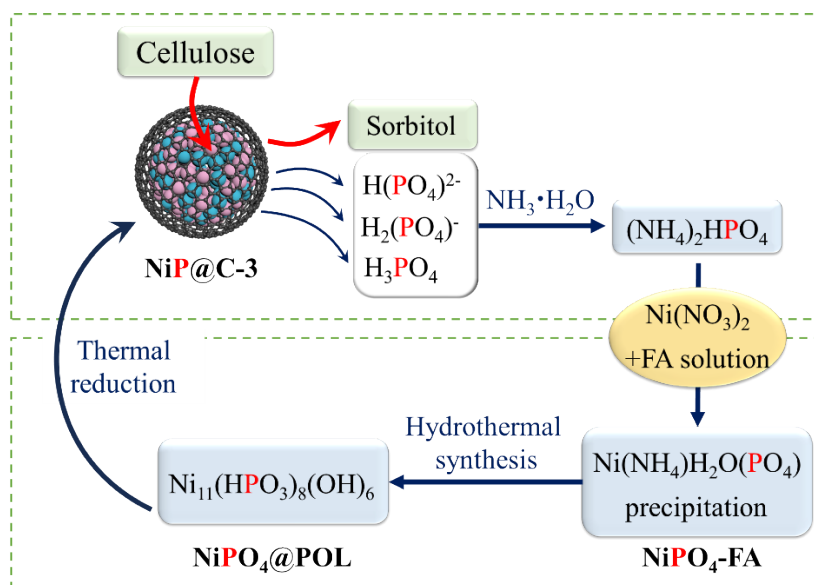


Fig. S27. Scheme of preparation, recycle, and regeneration of catalyst.

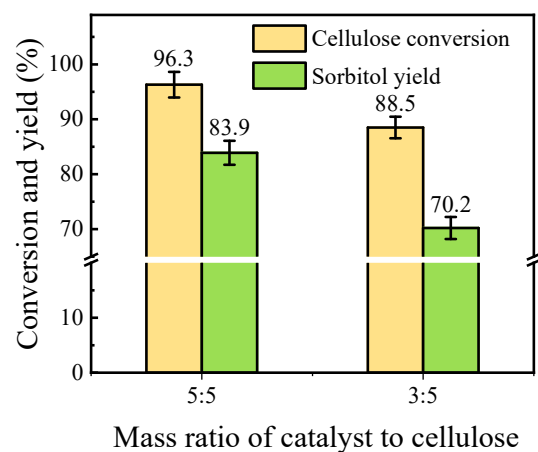


Fig. S28. Catalytic performance for two catalyst-cellulose ratios (reaction condition: 50 mg cellulose, 50 mg catalyst (5:5) or 30 mg catalyst (3:5), 5 mL H₂O, 200 °C reaction temperature, 4 MPa partial pressure H₂, 3 h reaction time).

References

1. Kresse and Hafner, *Physical review. B, Condensed matter*, 1993, **47**, 558-561.
2. Kresse and Hafner, *Physical review. B, Condensed matter*, 1994, **49**, 14251-14269.
3. G. Kresse and J. Furthmüller, *Comput. Mater. Sci*, 1996, **6**, 15-50.
4. Kresse and Furthmuller, *Physical review. B, Condensed matter*, 1996, **54**, 11169-11186.
5. Blochl, *Physical review. B, Condensed matter*, 1994, **50**, 17953-17979.
6. G. Kresse and D. Joubert, *Physical Review B*, 1999, **59**, 1758-1775.
7. Perdew, Burke and Ernzerhof, *Phys. Rev. Lett.*, 1996, **77**, 3865-3868.
8. S. Grimme, J. Antony, S. Ehrlich and H. Krieg, *The Journal of Chemical Physics*, 2010, DOI: 10.1063/1.3382344.
9. J. Rossmeisl, A. Logadottir and J. K. Nørskov, *Chem. Phys.*, 2005, DOI: 10.1016/j.chemphys.2005.05.038.
10. P. Pachfule, D. Shinde, M. Majumder and Q. Xu, *Nature chemistry*, 2016, **8**, 718-724.